Article

Antibacterial and Cytotoxicity of Extracts and Isolated Compounds from *Artemisia abyssinica*: A Combined Experimental and Computational Study

Dawit Tesfaye, Milkyas Endale, Venkatesha Perumal Ramachandran, Emebet Getaneh, Guta Amenu, Leta Guta, Taye B. Demissie, Japheth O. Ombito, Rajalakshmanan Eswaramoorthy, and Yadessa Melaku*

Read Online

ACCESS | Metrics & More | Article Recommendations | SI Supporting Information

ABSTRACT: *Artemisia abyssinica* is a widely cultivated hedge plant in Ethiopia. Traditionally, they have been used to treat a variety of health conditions, including intestinal problems, infectious diseases, tonsillitis, and leishmaniasis. Silica gel chromatographic separation of the methanol and ethyl acetate extracts of the leaves, roots, and stem barks of *A. abyssinica* led to the isolation of 12 compounds, labeled as 1−12. Among these, compounds 1, 3, 4, 5, and 7−11 are reported as new to the genus *Artemisia*. The extracts and isolated compounds from *A. abyssinica* were evaluated for their in vitro antibacterial activity against four bacterial strains: *Streptococcus pyogenes*, *Staphylococcus aureus*, *Pseudomonas aeruginosa*, and *Escherichia coli*, using the disc diffusion assay. All of the extracts displayed weak antibacterial activity, with inhibition zone diameters (IZDs) ranging from 6.10 ± 0.3 to 9.30 ± 0.20 mm. The isolated compounds, on the other hand, exhibited weak to moderate

antibacterial activity, with IZDs ranging from 6.00 ± 0.300 to 13.50 ± 0.50 mm. The most potent antibacterial activity was observed for compound 6, which showed an IZD of 13.30 ± 0.50 mm against *E. coli* and 13.50 ± 0.50 mm against *P. aeruginosa*. This activity was comparable to that of the positive control ceftriaxone, which had IZDs of 14.1 ± 0.3 and 13.8 ± 0.5 mm against *E. coli* and *P. aeruginosa*, respectively. The in silico molecular docking analysis against DNA gyrase B revealed that compound 5 showed a higher binding affinity (-6.9 kcal/mol), followed by compound 10 (-6.7 kcal/mol) and compound 12 (-6.3 kcal/mol), whereas ciprofloxacin showed -7.3 kcal/mol. The binding affinities of compounds 5, 11, 10, and 9 were found to be -5.0, -4.3, -4.2, and -4.0 kcal/mol against *S. aureus* Pyruvate kinase, respectively, whereas ciprofloxacin showed a binding affinity of -4.9 kcal/mol, suggesting that compound 5 had a better binding affinity compared with ciprofloxacin. The effect of extracts of *A. abyssinica* was evaluated for cytotoxic activity against the breast cancer cell line (MCF-7) by the MTT assay. The extracts induced a decrease in cell viability and exerted a cytotoxic effect at a concentration of 20 μg/mL. The highest percent cell viability was observed for the methanol extract of the stem (92.9%), whereas the least was observed for the methanol extract of the root (34.5%). The result of the latter was significant compared with the positive control. The binding affinities of the isolated compounds were also assessed against human topoisomerase inhibitors IIβ. Results showed that compound 5 showed a binding affinity of -6.0 kcal/mol, followed by 11 (-5.4 kcal/mol), 10 (-5.0 kcal/mol), and 11 (-4.9 kcal/mol). Similar to ciprofloxacin, compounds 4, 5, 6, 9, 10, and 12 comply with Lipinski's rule of five. Overall, the comprehensive investigation of the chemical constituents and their biological activities reinforces the traditional medicinal applications of *A. abyssinica* and warrants further exploration of this plant as a source of novel therapeutic agents.
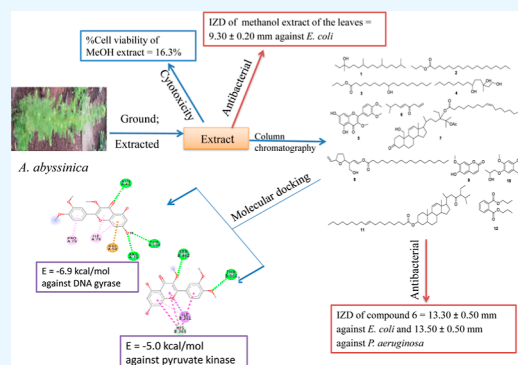
1. INTRODUCTION

The genus *Artemisia* in the family Asteraceae consists of over 500 species geographically distributed all over the world except Antarctica.[1] Species of this genus can be perennial, biennial or annual grasses, shrubs or bushes that are generally aromatic, with erect or ascending stems.[2] *Artemisia* species have a wide range of uses in folk medicine and have been the subject of numerous chemical and biological studies.[3] The genus has been reported to be rich in various secondary metabolites such as flavonoids,

lignans, sesquiterpene lactones, coumarins, caffeoylquinic acids, acetylenes, and sterols,[4] which possess various biological

activities including diuretic,[5] antimalarial, antimicrobial, antiviral, anthelmintic, anti-inflammatory, bronchodilator, hypolipidemic, antihypertensive, antioxidant, immunomodulatory, cytotoxic, antitumor, and laxative.[6,7]

Cancer is a disease characterized by abnormal cell division and proliferation that results from the disruption of molecular signals that control these processes. The prevalence of this disease is rising rapidly in Africa, Asia, and Central and South America, which in fact account for about 70% of cancer deaths in the world. The most commonly diagnosed cancer is female breast cancer, followed by lung cancer.[8−10] Previous studies on *Artemisia* species have shown medicinal properties, such as antibacterial and anticancer effects. Many phytochemicals exert their cytotoxic effects by acting as cell cycle and apoptosis regulators, as well as anti-inflammatory agents.[9]

Artemisia abyssinica Sch. Bip. ex A. Rich is an aromatic, gray, silky-hairy plant with pale yellow flower-heads and is well-known as a stimulant and an analgesic.[11] The plant has been used as an anthelmintic, antispasmodic, antirheumatic, and antibacterial agent.[12] The aforementioned uses could be attributed to the presence of various secondary metabolites such as alkaloids, flavonoids, sterols, tannins, anthraquinones, and volatile oils.[13] The plant is a popular hedge plant in Ethiopia and is traditionally used for intestinal problems, infectious diseases, and as an antileishmanial.[14] The whole herb is employed to alleviate tonsillitis, and a traditional infusion is consumed as a remedy for colds and illnesses in children.[15] Despite the tremendous traditional uses of the plant against various arrays of diseases, there are limited previous studies of the chemistry and biological activities of this species. Hence, in this paper, a comprehensive investigation of the chemical constituents, antibacterial activities, and in silico molecular docking analysis of extracts and compounds isolated from *A. abyssinica* is presented.

2. MATERIALS AND METHODS

2.1. Plant Material Collection, Authentication, and Preparation. The whole plant of *A. abyssinica* was collected from Tiyo Woreda, Arsi zone [7°57′N 39°7′E/7.95°N 39.117°E/7.95] southeastern Ethiopia with an elevation of 2430 m[16] on July 2020. The specimen was authenticated by Mr. Wege Abebe of Adiss Ababa University, and the voucher specimen was deposited in the National Herbarium, Addis Ababa University (Code: G-003). The plant material was washed with distilled water, air-dried, powdered using a milling machine, and then stored in a polyethylene bag in a refrigerator.

2.2. Extraction. The air-dried and powdered leaves, stems, and roots (each 300 g) of *A. abyssinica* were extracted successively by maceration using *n*-hexane (each 1.5 L), ethyl acetate (each 1.5 L), and methanol (each 1.5 L) at room temperature for 72 h. Removal of the solvent at 40 °C under reduced pressure gave 1 g (0.3%) *n*-hexane, 5.3 g (1.8%) EtOAc, and 11.3 g (3.8%) MeOH extracts for the leaves; 0.8 g (0.27%) *n*-hexane, 3.5 g (3.5%) EtOAc, and 10.2 g (4.4%) MeOH extract for the stems; and 0.6 g of *n*-hexane (0.2%), 1.1 g (0.7%) EtOAc, and 5.1 g (1.7%) MeOH extracts for the roots. Analysis using TLC showed that the EtOAc and methanol extracts had similar spots and were hence combined for the isolation of compounds.

2.3. Isolation. The combined extract of the leaves of *A. abyssinica* (16 g) was adsorbed on silica gel (12 g) and subjected to silica gel column chromatography over silica gel (240 g) eluted by increasing the gradient of EtOAc in *n*-hexane to afford 230 fractions, 10 mL each. **Fractions 1−10** (10%) EtOAc in *n*-hexane were subjected to silica gel column chromatography to

afford 12 subfractions, each 10 mL. **Subfractions 8−10** were identified as compound **1** (53 mg). **Fractions 17−24** (20% EtOAc in *n*-hexane) after silica gel column chromatography afforded 8 subfractions, each 10 mL. **Subfractions 4−7** were identified as compound **2** (30 mg). **Fractions 25−47** (20% EtOAc in *n*-hexane) were fractionated over silica gel column chromatography to afford 12 subfractions, each 10 mL. Subfractions 5−10 were identified as compound **3** (51 mg). **Fractions 81−95** (30% EtOAc in *n*-hexane) were combined and rechromatographed to afford 6 subfractions, each 10 mL. **Subfractions 4−6** were identified as compound **4** (20.6 mg). **Fractions 190−199** (90% EtOAc in *n*-hexane) were subjected to silica gel column chromatography to afford 11 subfractions, each 10 mL. **Subfractions 7−11** and subfraction 12 were identified as compounds **5** (33 mg) and **6** (21 mg).

The combined extract of the stem of *A. abyssinica* (13 g) was adsorbed with the same amount of silica gel and subjected to column chromatography over silica gel (220 g) using *n*- hexane: EtOAc of increasing polarity afforded 200 fractions, 10 mL each. **Fractions 11−30** (20% EtOAc in *n*-hexane), after silica gel column chromatography, afforded 16 subfractions, each 10 mL, from which subfractions 6−14 and subfractions 15−16 were identified as compounds **7** (20 mg) and **8** (15 mg), respectively. **Fractions 141−152**, eluted using *n*-hexane: EtOAc (4:1), were subjected to silica gel column chromatography to afford 20 subfractions, each 10 mL, and subfractions 11−18 yielded compound **9** (22 mg). Fractions F121−F130 (0.5 g) were eluted using 40% EtOAc in *n*-hexane (6:4) after silica gel column chromatography to afford 15 subfractions, each 10 mL, and subfractions 7−15 were identified as compound **10** (30 mg).

The combined extract of the root of *A. abyssinica* (6 g) was adsorbed on silica gel (10 g) and subjected to silica gel column chromatography over silica gel (230 g) using *n*-hexane: EtOAc of increasing polarity to afford 200 fractions, 10 mL each. **Fractions 11−20** (20% EtOAc in *n*-hexane) were fractionated over silica gel column chromatography to afford 8 fractions, each 10 mL, while fractions 3−6 gave compound **11** (35 mg). **Fractions 25−30** (20% EtOAc in *n*-hexane) were rechromatographed over silica gel to afford 9 subfractions, each 10 mL, from which subfractions 4−7 were identified as compound **12** (40 mg).

2.4. In Vitro Biological Activity. *2.4.1. Cytotoxicity Assay.* MCF-7 breast cancer cell lines were obtained from NCCS (National Center for Cell Science), Pune, India. The cells were maintained at 37 °C in a humidified atmosphere with 5% CO_2. Upon reaching confluency, the cells were trypsinized and passaged to be used for further assays. The antiproliferative effect of the extracts of *A. abyssinica* (20 μg each) was studied on human breast cancer cell lines (MCF-7); doxorubicin was used as a positive control. The cells were grown in T25 culture flasks containing DMEM and L-15 supplemented with 10% FBS and 1% antibiotics (100 μg mL^{-1} penicillin and 100 μg mL^{-1} streptomycin). The cells were maintained at 37 °C in a humidified atmosphere containing 5% CO_2. Upon reaching confluence, the cells were detached using a Trypsin−EDTA solution and were subcultured at a density of 5000 cells per well. At 50% confluence, the culture medium was aspirated, and the cells were treated with 20 μg of plant extract in DMSO (20 μL) for 24 h at 37 °C in the CO_2 incubator. Later, cells were incubated with MTT (4 mg mL^{-1}) for 3 h. The absorbance was measured at 540 nm with a standard microplate reader. The experiments were done in triplicate, and the results were reported as the M ± SD.
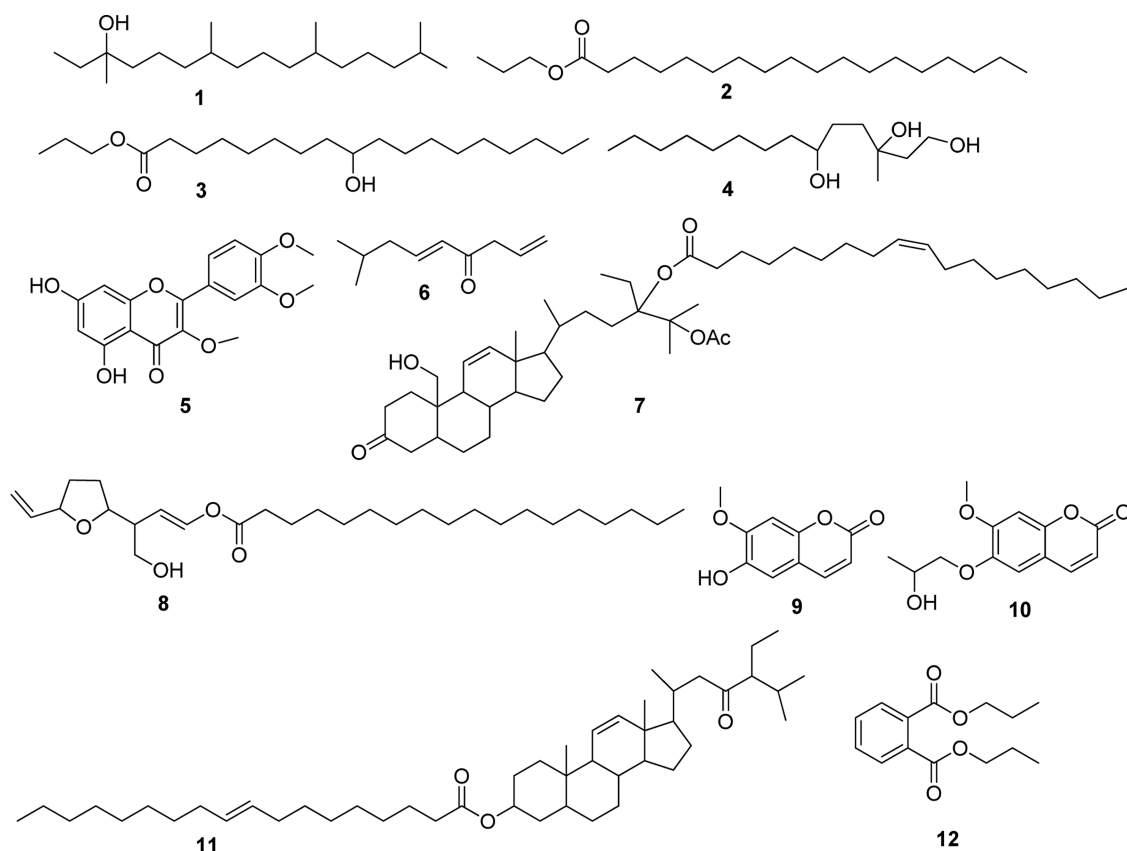
Figure 1. Compounds isolated from *Artemisia abyssinica*.

2.4.2. Antibacterial Activity. The antibacterial activity of the extracts and isolated compounds was evaluated using a disc diffusion assay.[17] Clinical bacterial strains with American standards, including *Escherichila coli* (ATCC 25922), *Pseudomonas aeruginosa* (ATCC 27853), *Staphylococcus aureus* (ATCC 25923), and *Staphylococcus pyogens* (ATCC 19615), were obtained from the Oromia Regional Laboratory and Quality Control, Adama, Ethiopia. McFarland number 0.5 standard was prepared by mixing 9.95 mL 1% H_2SO_4 in distilled water and 0.05 mL 1% $BaCl_2$ in distilled water to estimate bacterial density.[18] The prepared sample was stored in an airtight bottle and used for comparison of bacterial suspension. Extracts and isolated compounds were prepared in DMSO to give 30, 15, 7.5, and 3.75 μg/mL concentrations. Bacteria cell suspensions were adjusted to the 0.5 McFarland turbidity standard to prepare a 1.5 × 10^8 CFU/mL inoculum. Each bacterial suspension was inoculated on Mueller−Hinton agar plates, and the plates were allowed to dry for 5 min. The sterile filter paper disks (6 mm in diameter) were soaked in 30, 15, 7.5, and 3.75 μg/mL concentrations of the crude extracts and isolated compounds. The extracts and isolated compounds soaked in filter paper disks were placed on the inoculated Mueller−Hinton agar plates, and the analyses were conducted in triplicate. Ciprofloxacin (CPFX, 30 μg/mL) disk was used as the positive control, and DMSO was used as the negative control. The plates were incubated for 18 h at 35 ± 2 °C. After incubation, the zones of inhibition were recorded as the diameter of the growth-free zones measured in mm using an antibiotic zone reader. The experiments were done in triplicate, and the results were reported as the M ± SD.

3. METHODOLOGY

3.1. Computational Study. The test compounds were subjected to computational studies to predict their drug-likeness property, viz., Lipinski's rule of five (ROF),[19] Veber rule,[20] pharmacokinetics, and drug-likeness using SwissADME,[21] PreADMET,[22] and in silico cytotoxicity using ProTox-II[23] online tools.

3.2. In Silico Molecular Docking. The test compounds' chemical structures were drawn using ACD/ChemSketch, and Gaussian09[24] software was used to optimize the structures by the DFT/B3LYP[25] technique, utilizing basis sets of 6-31G-(d,p).[25] The energy-minimized ligands were then put into the docking procedure. The binding site attributes: center_x = 61.680259; center_y = 28.330852; center_z = 64.290148; and size_x; size_y; size_z = 20. The targets, *Escherichia coli* DNA gyrase (PDB ID: 6F86), *S. aureus* Pyruvate kinase (PK) (PDB ID: 3T07), and Human topoisomerase IIβ were retrieved from the Protein Data Bank (https://www.rcsb.org/). For the docking studies, *S. aureus* PK (PDB ID: 3T07) was used as a target, and CPFX was used as a reference control. Binding site attributes: center_x = −12.446889; center_y = 0.983556; center_z = 2.585889; and size_x; size_y; size_z = 20. Biovia Discovery Studio 2020 was used to prepare the targets.[26] The protein complex's water molecules were removed, and the bound ligand was chosen to determine the characteristics of the binding sites before being removed from the complex.[27] Validation of the binding sites was done by redocking the bound ligand with the target protein.[28] The target was augmented with polar hydrogen atoms and the necessary charges. Using AutoDoc Vina (MGLTools-1.5.6), the target and ligand were generated in the necessary format (pdbqt) for

docking, and docking was performed.[27] Hundred conformers and their associated binding energies were generated for each ligand during the docking procedure.[29] Using Biovia Discovery Studio 2020, the receptor and ligand interactions were ascertained by selecting the conformation with the lowest binding energy. In the present study, human TOP2β (PDB ID: 3QX3) was used as a target, and EVP was used as a reference control. Binding site attributes: center_x = 33.025762; center_y = 95.765381; center_z = 51.567476; size_x; size_y; size_z = 20.

4. RESULTS AND DISCUSSION

Silica gel chromatographic fractionation of various parts of the extracts of *A. abyssinica* has led to the isolation of 12 compounds (Figure 1). The detailed structural elucidations were presented as follows.

Compound **1** was obtained as a white solid from the combined ethyl acetate and methanol extracts of the leaves of *A. abyssinica*. The ^{1}H NMR spectrum (Figure S1) revealed signals in the region δ_H 1.2 to 0.80. The signal observed at δ_H = 0.80 is due to methyl protons. The ^{13}C NMR spectrum (Figure S2) showed a signal due to sp[3] quaternary oxygenated carbon at δ_C 77.2 and methyl carbon peaks at δ_C 32.9, 32.8, and 32.7. The remaining signals at δ_C 31.9, 29.7, 26.7, 29.6, 29.4, 27.1, and 22.7 were due to methylene carbons, which were supported by the DEPT-135 spectrum (Figure S3). The above spectral data, is in good agreement with previous reports,[30] suggesting the compound a diterpene named 3,7,11,15-tetramethylhexadecan-3-ol reported from this species for the first time. The structure of the compound was also confirmed by [1]H−^{1}H COSY and HMBC spectra (Figure S4).

Compound **2** was obtained as a white solid from the combined ethyl acetate and methanol extracts of the leaves of *A. abyssinica*. The ^{1}H NMR spectrum (Figure S5) revealed oxymethylene signals at δ_H 3.98 (2H, t, *J* = 6.4 Hz), methylene attached to carbonyl at δ_H 2.22, and terminal methyl protons at δ_H 0.8 (3H). The ^{13}C NMR spectrum with the aid of the DEPT-135 (Figures S6 and S7) showed diagnostic signals due to ester carbonyl and oxymethylene at δ_C 174.1 and 64.4, respectively. The signal characteristics of methylene adjacent to carbonyl carbon appeared at δ_C = 34.4. The above spectral data, along with the literature reported for the same compound,[31] suggest that compound **2** is identical with a fatty acid ester named propyl stearate. This was confirmed by the spectral data obtained from [1]H−^{1}H COSY and HMBC (Figure S8).

Compound **3** was isolated as a white solid from combined ethyl acetate and methanol extracts of the leaves of *A. abyssinica*. The ^{1}H NMR spectrum (Figure S9) revealed an sp[3] oxygenated methine signal at δ_H 4.42 (1H, m), oxymethylene at δ_H 4.20 (2H, t, *J* = 6.4 Hz), methylene attached to carbonyl at δ_H 2.44 (2H), and terminal methyl protons at δ_H 0.81. The ^{13}C NMR spectrum with the aid of the DEPT-135 spectrum (Figures S10 and S11) showed signals at δ_C 174.1, 63.1, 81.0, 34.4, and 14.1 due to ester carbonyl, oxymethylene, sp[3] oxygenated methine, and methylene attached to carbonyl and terminal methyl carbons, respectively. The spectrum also displayed signals due to aliphatic methylenes at δ_C = 34.4, 32.8, 32.0, 29.7, 29.6, 29.4, and 22.7. Compound **3** is the same as compound **2**, except for the presence of a hydroxyl group at C-9. Hence, compound **3** is identified as a fatty acid ester named propyl-9-hydroxyoctadecanoate. The [1]H−^{1}H COSY (Figure S12) and HMBC spectra also confirm the assertion.

Compound **4** was isolated as a white solid from the combined ethyl acetate and methanol extracts of the leaves of *A. abyssinica*.

The ^{1}H NMR spectrum of compound **4** (Figure S13) revealed a signal at δ_H 3.62 (3H, m) for methine and δ_H 3.60 (2H, m) for methylene protons attached to carbon connected to a hydroxyl group. Signals due to methylene protons were observed in the region between δ_H 1.3 to 1.6. The signal due to terminal methyl was evident at δ_H = 0.9 (3H, t). The ^{13}C NMR spectrum with the aid of the DEPT-135 spectrum (Figures S14 and S15) showed peaks at δ_C 81.7, 72.5, 63.0, and 13.1 due to sp3 quaternary, oxymethylene, and terminal methyl carbons, respectively. Other signals were evident at δ_C 35.2, 31.7, 29.4, 29.3, 29.2, 29.2, 29.1, 29.0, 28.2, 27.5, and 22.4. The above spectral data, along with the literature report, suggest that compound **4** is a terpene, 3-methyltetradecane-1,3,6-triol. This was further established by the [1]H−^{1}H COSY and HMBC correlations of the compound (Figure S16).

Compound **5** was isolated as a brown crystal from the combined ethyl acetate and methanol extracts of the leaves of *A. abyssinica*. The compound melted at 240−242 °C (lit. 242−245).[31] The ^{1}H NMR spectrum of compound **5** (Figure S17) revealed signals due to meta-coupled protons at δ_H 6.7 (1H, d, *J* = 2.4 Hz) and 6.4 (1H, d, *J* = 2.4 Hz) with an AB spin pattern, along with three aromatic protons at δ_H 7.7 (1H, m), 7.1 (1H, d), and 7.7 (1H, m) with an ABX spin pattern attributed to rings A and B of flavonoid skeleton, respectively. Signals at δ_H = 4.0 (3H, s), 3.9 (3H, s), and 3.8 (3H, s) suggest the presence of three methoxy groups. The ^{13}C NMR spectrum with the aid of the DEPT-135 spectrum (Figures S18 and S19) showed carbonyl carbon at δ_C 178.7 (C-4), and sp[2] oxygenated quaternary carbons at δ_C 165.9 (C-7), 161.4 (C-5), 156.9 (C-8a), 156.7 (C-2), 149.8 (C-4′), 147.6 (C-5′), and 138.4 (C-3). Signals due to two sp[2] aromatic quaternary species were observed at δ_C 122.4 (C-1′) and 105.4 (C-4a), along with five sp[2] methine carbons at δ_C 122.4 (C-2′), 115.0 (C-3′), 111.5 (C-6′), 97.6 (C-6), and 91.8 (C-8). The above spectral data, along with comparison with the literature report, suggest that compound **5** is a flavonoid named quercetin 3,3,4′-trimethyl ether.[32] The structure of compound **5** was also confirmed by 2D NMR, including COSY and HMBC (Figure S20).

Compound **6** was isolated as a brown crystalline solid from the combined ethyl acetate and methanol extracts of the leaves of *A. abyssinica*. The ^{1}H NMR spectrum of compound **6** (Figure S21) revealed the presence of five olefinic protons at δ_H 6.92 (1H, m), 6.09 (1H, m), 5.96 (1H, m), 5.28 (1H, m), and 5.12 (1H, m). The ^{13}C NMR (Figure S22) spectrum demonstrated the presence of nine carbon signals of which the most downfield signal at δ_C 199.8 is attributed to carbonyl carbon, whereas sp2 methine carbons were evident at δ_C 145.2, 144.4, 133.2, and 111.3. The latter is due to terminal methylene carbon (Figure S23). Two methylene carbons were observed at δ_C 44.8 and 29.4, supported by the DEPT-135 spectrum. Signals at δ_C 26.4 and 25.3 belong to the sp[3] methine and methyl carbons, respectively. Based on the above spectral data along with the COSY and HMBC spectra (Figure S24), compound **6** is suggested as 8-methylnona-1,5-dien-4-one[6].

Compound **7** was isolated as a white crystalline from the combined ethyl acetate and methanol extracts of the stem of *A. abyssinica*. The UV−vis spectrum of compound **7** revealed an absorption maxima at 205 nm (Figure S25), suggesting the absence of conjugation in the structure. The ^{1}H NMR spectrum of compound **7** (Figure S26) revealed signals due to olefinic protons at δ_H 5.72 (2H, s), 5.16 (1H, m), and 5.04 (1H, m). The spectrum displayed a signal due to oxymethine at δ_H 3.6 (2H). The proton decoupled ^{13}C NMR spectrum of compound **7**

Table 1. Antibacterial Activity of Constituents of *A. abyssinica*[a]

samples	concentration (μg/mL)	zone of inhibition (mm)			
		E. coli	P. aerugisnosa	S. aureus	S. pyogens
CAALM	30	9.30 ± 0.20	8.00 ± 0.20	8.50 ± 0.20	8.10 ± 0.20
	15	8.80 ± 0.30	7.20 ± 0.30	7.90 ± 0.30	7.90 ± 0.30
	7.5	7.30 ± 0.10	7.00 ± 0.10	7.30 ± 0.10	7.30 ± 0.10
	3.25	6.90 ± 0.20	6.90 ± 0.20	6.70 ± 0.20	6.90 ± 0.20
	1.625	6.50 ± 0.40	6.40 ± 0.40	6.60 ± 0.40	6.50 ± 0.40
CAASM	30	7.40 ± 0.40	7.80 ± 0.20	8.10 ± 0.20	7.40 ± 0.30
	15	7.00 ± 0.30	7.40 ± 0.30	7.10 ± 0.10	7.00 ± 0.30
	7.5	6.80 ± 0.10	6.60 ± 0.20	6.90 ± 0.10	6.90 ± 0.20
	3.25	6.50 ± 0.10	6.30 ± 0.20	6.70 ± 0.30	6.50 ± 0.20
	1.625	6.30 ± 0.40	6.10 ± 0.30	6.40 ± 0.40	6.30 ± 0.50
CAARM	30	8.80 ± 0.20	9.00 ± 0.20	7.30 ± 0.20	7.10 ± 0.20
	15	8.60 ± 0.30	7.20 ± 0.30	6.80 ± 0.30	7.00 ± 0.30
	7.5	7.30 ± 0.10	7.00 ± 0.20	6.60 ± 0.10	6.80 ± 0.10
	3.25	6.90 ± 0.20	6.60 ± 0.30	6.60 ± 0.20	6.90 ± 0.40
	1.625	6.50 ± 0.40	6.40 ± 0.50	6.50 ± 0.40	6.10 ± 0.40
1	30	6.50 ± 0.20	8.50 ± 0.80	6.40 ± 0.20	7.00 ± 0.20
	15	6.40 ± 0.30	6.30 ± 0.20	6.40 ± 0.20	6.90 ± 0.30
	7.5	6.30 ± 0.20	6.50 ± 0.40	6.30 ± 0.20	6.80 ± 0.30
	3.25	6.20 ± 0.30	6.30 ± 0.10	±0.10	6.30 ± 0.20
	1.625	6.10 ± 0.20	6.10 ± 0.10	6.10 ± 0.20	6.10 ± 0.30
2	30	7.20 ± 0.30	8.40 ± 0.30	6.60 ± 0.20	8.80 ± 0.60
	15	6.60 ± 0.30	6.80 ± 0.50	6.50 ± 0.10	7.00 ± 0.50
	7.5	6.70 ± 0.20	6.70 ± 0.40	6.30 ± 0.10	6.80 ± 0.50
	3.25	6.40 ± 0.40	±0.10	6.20 ± 0.10	6.20 ± 0.20
	1.625	6.20 ± 0.20	6.10 ± 0.10	6.10 ± 0.20	6.10 ± 0.20
3	30	11.5 ± 0.30	10.1 ± 0.50	7.0 ± 0.30	10.5 ± 0.50
	15	11.1 ± 0.30	8.3 ± 0.50	6.9 ± 0.30	8.4 ± 0.50
	7.5	9.9 ± 0.40	7.3 ± 0.30	6.6 ± 0.10	7.0 ± 0.60
	3.25	7.7 ± 0.30	6.6 ± 0.20	6.2 ± 0.20	6.2 ± 0.30
	1.625	6.8 ± 0.20	6.3 ± 0.20	6.1 ± 0.20	6.1 ± 0.20
4	30	12.1 ± 0.30	12.9 ± 0.90	12.7 ± 0.90	10.8 ± 1.10
	15	11.1 ± 0.10	10.9 ± 0.90	11.6 ± 0.70	8.0 ± 0.80
	7.5	10.3 ± 0.20	10.0 ± 0.90	9.3 ± 0.70	7.4 ± 0.80
	3.25	8.1 ± 0.30	8.3 ± 0.40	8.1 ± 0.60	6.1 ± 0.20
	1.625	6.8 ± 0.30	7.8 ± 0.20	8.0 ± 0.20	6.0 ± 0.20
5	30	7.8 ± 0.30	8.7 ± 0.30	6.6 ± 0.40	7.9 ± 0.40
	15	7.6 ± 0.40	7.5 ± 0.20	6.5 ± 0.10	7.5 ± 0.20
	7.5	7.5 ± 0.30	7.2 ± 0.40	6.4 ± 0.40	6.9 ± 0.20
	3.25	6.4 ± 0.30	7.3 ± 0.60	6.2 ± 0.30	6.5 ± 0.10
	1.625	6.2 ± 0.30	6.8 ± 0.50	6.1 ± 0.30	6.3 ± 0.30
6	30	13.3 ± 0.50	13.5 ± 0.50	7.9 ± 0.30	11.4 ± 0.40
	15	11.3 ± 0.40	11.6 ± 0.40	7.1 ± 0.50	8.5 ± 0.40
	7.5	9.9 ± 0.60	9 ± 0.50	6.6 ± 0.40	7.7 ± 0.20
	3.25	7.1 ± 0.30	7.0 ± 0.20	6.5 ± 0.60	6.7 ± 0.30
	1.625	6.8 ± 0.40	6.8 ± 0.40	6.3 ± 0.30	6.5 ± 0.30
7	30	8.2 ± 0.10	8.2 ± 0.60	6.9 ± 0.30	6.7 ± 0.20
	15	7.6 ± 0.30	6.6 ± 0.10	6.6 ± 0.30	6.4 ± 0.20
	7.5	7.1 ± 0.30	7.5 ± 0.90	6.6 ± 0.30	6.4 ± 0.30
	3.25	6.2 ± 0.20	6.7 ± 0.50	6.2 ± 0.20	6.2 ± 0.10
	1.625	6.0 ± 0.30	6.4 ± 0.30	6.1 ± 0.30	6.1 ± 0.30
8	30	6.8 ± 0.70	9.2 ± 0.50	8.1 ± 0.40	7.1 ± 0.50
	15	6.7 ± 1.00	8.6 ± 0.40	7.4 ± 0.10	6.8 ± 1.00
	7.5	6.6 ± 0.30	8.2 ± 0.80	6.9 ± 0.20	6.7 ± 0.30
	3.2	6.3 ± 0.50	7.5 ± 0.40	6.6 ± 0.30	6.4 ± 0.20
	1.625	6.1 ± 0.30	6.6 ± 0.30	6.3 ± 0.30	6.2 ± 0.10
9	30	8.1 ± 0.20	8.1 ± 0.30	7.5 ± 0.30	8.3 ± 0.30
	15	7.9 ± 0.30	7.6 ± 0.60	7.0 ± 0.50	7.4 ± 0.80
	7.5	7.3 ± 0.10	7.1 ± 0.80	6.8 ± 0.70	7.1 ± 1.00
	3.25	6.9 ± 0.20	7.0 ± 0.50	6.5 ± 0.50	7.0 ± 1.00

Table 1. continued

		zone of inhibition (mm)			
samples	concentration (μg/mL)	E. coli	P. aeruginsosa	S. aureus	S. pyogens
	1.625	8.1 ± 0.20	8.1 ± 0.30	7.5 ± 0.30	8.3 ± 0.30
10	30	8.3 ± 0.30	7.1 ± 0.50	8.2 ± 0.50	9.1 ± 0.60
	15	7.7 ± 0.80	6.8 ± 0.30	7.6 ± 0.40	9.0 ± 0.50
	7.5	7.4 ± 1.00	6.5 ± 0.30	7.3 ± 0.50	8.0 ± 0.40
	3.25	6.9 ± 1.00	6.4 ± 0.50	7.0 ± 0.50	7.2 ± 0.30
	1.625	6.5 ± 0.20	6.3 ± 0.30	6.6 ± 0.20	7.0 ± 0.30
11	30	9.5 ± 0.20	8.1 ± 0.20	8.1 ± 0.40	8.1 ± 0.30
	15	9.3 ± 0.30	7.5 ± 0.40	7.9 ± 0.30	8.0 ± 0.20
	7.5	7.5 ± 0.20	7.1 ± 0.10	7.3 ± 0.10	7.6 ± 0.31
	3.25	6.8 ± 0.20	6.8 ± 0.50	6.9 ± 0.20	7.0 ± 0.30
	1.625	6.3 ± 0.50	6.5 ± 0.40	6.5 ± 0.40	6.9 ± 0.50
12	30	8.3 ± 0.30	8.1 ± 0.20	8.1 ± 0.20	8.1 ± 0.20
	15	7.6 ± 0.30	7.2 ± 0.30	7.9 ± 0.30	7.6 ± 0.30
	7.5	7.1 ± 0.20	6.9 ± 0.10	7.3 ± 0.10	7.3 ± 0.10
	3.25	6.8 ± 0.20	6.7 ± 0.20	6.9 ± 0.20	7.0 ± 0.20
	1.625	6.5 ± 0.50	6.5 ± 0.40	6.0 ± 0.40	6.5 ± 0.20
ceftriaxone	30	14.1 ± 0.30	13.8 ± 0.50	14.4 ± 0.90	16.2 ± 0.60

[a]CAALM (*A. abyssinica* leaves methanol extract), CAASM (*A. abyssinica* stem methanol extract), and CAARM (*A. abyssinica* root methanol extract).

analyzed with the aid of the DEPT-135 spectrum (Figures S27 and S28) showed signals at δ_C 199.8, 171.82, and 171.8 due to the presence of three carbonyl carbons, with the earlier due to ketone carbonyl. Signals due to the presence of four olefinic carbons were evident at δ_C 138.1, 129.5, 123.7, and 123.6. The presence of three oxygenated aliphatic carbons was observed at δ_C 81.1, 77.2, and 63.1. The DEPT-135 spectrum established the latter to be a methylene carbon, while the earlier two to be quaternary carbons. Other signals due to aliphatic carbons were observed in the region between δ_C 55.9 to 12.2. The COSY and HMBC spectra were also used to confirm the structure of compound **7** (Figure S28). Hence, compound **7** was identified as a steroid, namely, 3-(2-acetoxypropan-2-yl)-6-(2,3,4,5,6,7,8,9,10,13,14,15,16,17-tetradecahydro-10-(hydroxymethyl)-13-methyl-3-oxo-1*H*-cyclopenta[*a*]phenanthren-17-yl)heptan-3-yl oleate.

Compound **8** was isolated as a white solid from the methanol extracts of the stem of *A. abyssinica*. The UV−vis of compound showed λ_{max} at 207 nm (Figure S49) confirming the absence of a conjugated chromophore. The ^{1}H NMR spectrum of compound **8** (Figure S30) revealed signals due to five olefinic protons at δ_H 6.36 (1H, m), 5.89 (2H, m), and 5.40 (2H, m). The diagnostic signal due to proton on oxygenated carbons was at δ_H 4.45 (1H, m) and 4.42 (1H, m). The triplet signal at δ_H 2.36 is due to protons on carbon adjacent to carbonyl carbon. The intense peak at δ_H 1.12 is evidence of the presence of many overlapping methylenes. The signal at δ_H = 0.89 is assigned to terminal methyl protons. The ^{13}C NMR (Figures S31 and S32) spectrum of compound **8** showed a signal at δ_C 179.4 due to ester carbonyl carbon. Characteristic signals due to olefinic carbons were observed at δ_C 144.1, 133.1, 111.5, and 120.5, where the latter is due to terminal olefinic carbon. The spectrum also demonstrated the presence of oxygenated carbons at δ_C values of 74.3 and 66.0. The spectrum also showed signals due to aliphatic carbons in the region between δ_C 33.9 to 14.1. Hence, compound **8** is identified as a (*E*)-3-(tetrahydro-5-vinylfuran-2-yl)-4-hydroxybut-1-enyl octadecanoate.

Compound **9** was isolated as a pale yellow crystalline solid from the methanol extracts of the stem of *A. abyssinica,* which

melted at 201−203 °C (Lit. 201).[33] The UV−vis spectrum showed λ_{max} at 346 nm (Figure S33), which is diagnostic for the presence of conjugation. The ^{1}H NMR spectrum of compound **9** (Figure S34) revealed the presence of two ortho-coupled protons at δ_H values of 7.81 (1H, d, *J* = 9.2 Hz) and 6.15 (1H, d, *J* = 9.5 Hz). Two singlet aromatic signals were observed at δ_H 7.07 (1H) and 6.72 (1H). The proton-decoupled ^{13}C NMR spectrum of compound **9** analyzed with the aid of DEPT-135 spectrum (Figures S35 and S36) showed ten carbon resonances with the most downfield signal at δ_C 162.6 due to α,β conjugated carbonyl carbon. The presence of three oxygenated aromatic carbons is apparent at δ_C 151.1, 149.5, and 145.7. The spectrum displayed signals due to olefinic carbons at δ_C 111.7 and 145.6 due to carbons α and β being adjacent to the carbonyl carbon. The remaining signals at δ_C 111.3, 109.5, and 102.9 are due to aromatic methine carbons. Hence, compound **9** is identified as 5-hydroxy-6-methoxycoumarin.[34,35]

Compound **10** was obtained as a white solid from the methanol extracts of the stem of *A. abyssinica*. The UV−vis spectrum demonstrated absorption maxima at λ_{max} of 348 nm (Figure S37). The ^{1}H NMR spectrum of compound **10** (Figure S38) revealed signals due to *ortho*-coupled protons at δ_H = 7.89 (1H, d, *J* = 9.6 Hz) and 6.20 (1H, d, *J* = 9.6 Hz). Two singlet signals were evident at δ_H 7.15 (1H, s) and 6.77 (1H, s). The signal at δ_H 3.97 (3H, s) is due to methoxy protons, while that at δ_H 1.98 (3H) is due to methyl protons. The ^{13}C NMR spectrum of compound **10** analyzed with the aid of the DEPT-135 spectrum (Figures S39 and S40) showed resonances of 13 carbons. The signals at δ_C 161.9, 151.3, 149.7, 145.7, 145.3, 111.9, 111.1, 109.7, and 103.1 establish the skeleton of the compound as a coumarin. Furthermore, the spectrum had four additional signals at δ_H 66.5, 65.2, 56.3, and 20.9 due to oxygenated methine, oxygenated methylene, and methoxy and methyl groups, respectively. Hence, compound **10** is identified as 6-(2-hydroxypropoxy)-7-methoxy-2*H*-chromen-2-one.

Compound **11** was isolated as a white crystalline solid from the combined extract of the root of *A. abyssinica*. The compound displayed an absorption maxima at 206 nm (Figure S41). The ^{1}H NMR spectrum of compound **11** (Figure S42) revealed four

Cell viability dose response curve
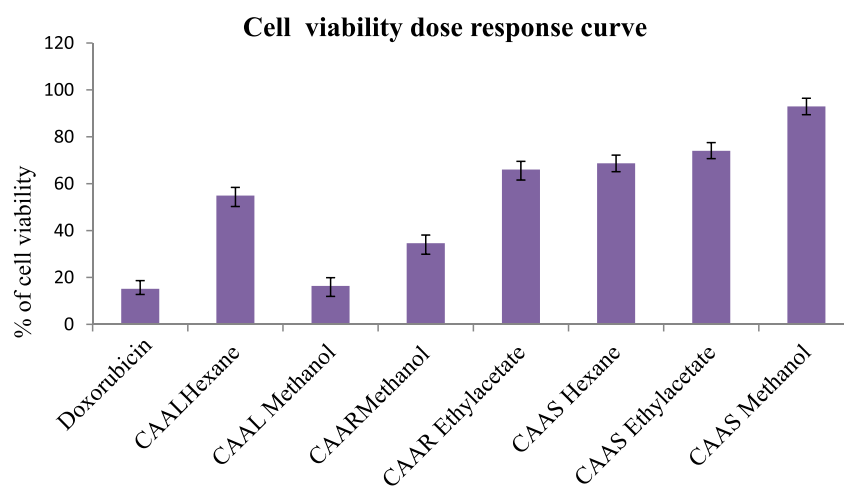
Figure 2. Cell viability test for the *A. abyssinica* extract. CAAL hexane: *A. abyssinicca* leaves hexane extract; CAAL methanol: *A. abyssinicca* leaves methanol extract; CAAR methanol: *A. abyssinicca* root methanol extract; CAAR ethyl acetate: *A. abyssinicca* root ethyl acetate extract; CAAS hexane: *A. abyssinicca* stem hexane extract; CAAS ethyl acetate: *A. abyssinicca* stem ethyl acetate extract; and CAAS methanol: *A. abyssinicca* stem methanol extract.

Table 2. Drug-Likeness Predictions of the Test and Standard Compounds Calculated by SwissADME[a]

C.no	formula	Mol. Wt. (g/mol)	NHD	NHA	LogP (cLogP)	Lipinski's ROF violation	NRB	TPSA (Å^2)	Veber's rule violation
1	$C_{20}H_{42}O$	298.55	1	1	6.32	1	13	20.23	1
2	$C_{21}H_{42}O_2$	326.56	0	2	6.98	1	19	26.3	1
3	$C_{21}H_{42}O_3$	342.56	1	3	6.03	1	19	46.53	1
4	$C_{15}H_{32}O_3$	260.41	3	3	3.17	0	12	60.69	1
5	$C_{18}H_{16}O_7$	344.32	2	7	2.54	0	4	98.36	0
6	$C_{10}H_{16}O$	152.23	0	1	2.66	0	5	17.07	0
7	$C_{49}H_{82}O_6$	767.17	1	6	10.75	2	26	89.9	1
8	$C_{28}H_{50}O_4$	450.69	1	4	7.24	1	22	55.76	1
9	$C_{10}H_8O_4$	192.17	1	4	1.51	0	1	59.67	0
10	$C_{13}H_{14}O_5$	250.25	1	5	1.78	0	4	68.9	0
11	$C_{47}H_{80}O_3$	693.14	0	3	12.01	2	23	43.37	1
12	$C_{14}H_{18}O_4$	250.29	0	4	3.05	0	8	52.6	0
CPFX	$C_{17}H_{18}FN_3O_3$	331.34	2	6	1.1	0	3	74.57	0

[a]NHD = number of hydrogen donor, NHA = number of hydrogen acceptor, NRB = number of rotatable bonds, and TPSA = total polar surface area.

signals in the olefinic regions at δ_H 5.75 (2H, s), 5.16 (1H, dd, *J* = 8.0 and 12.0 Hz), and 5.04 (1H, dd, *J* = 8.0 and 12.0 Hz). The signal due to the oxymethine proton is evident at δ_H 4.20 (1H, m). The proton decoupled ^{13}C NMR (Figures S43 and S44) spectrum of compound **11** displayed diagnostic signals due to the ketone carbonyl at δ_C 199.7. The presence of an ester carbonyl was also observed at δ_C 171.8. Four olefinic signals were observed at δ_C 138.1, 129.5, 123.8, and 123.7. The spectrum displayed a signal due to oxymethine carbon at δ_C 77.2. Characteristic signals of the steroid skeleton were observed in the region δ_C 56.0 to 12.3. Hence, compound **11** is a steroid identified as (9E)-17-(5-ethyl-6-methyl-4-oxoheptan-2-yl)-2,3,4,5,6,7,8,9,10,13,14,15,16,17-tetradecahydro-10,13-dimethyl-1*H* cyclopenta[*a*]phenanthren-3-yl-octadec-9-enoate.[36]

Compound **12** was obtained as a white crystalline solid melted at 317−319 °C. The UV−vis spectrum showed λ_{max} 210 and 275 nm (Figure S45). The ^{1}H NMR spectrum of compound **12** (Figure S46) revealed signals due to aromatic protons at δ_H 7.5 (2H, m) and 7.7 (2H, m). A signal due to oxymethylene was observed at δ_H 4.20 (4H, t). The ^{13}C NMR (Figures S47 and 48) spectrum of compound **12** showed a signal due to ester carbonyl at δ_C 167.6. Other aromatic carbons were observed at δ_C 132.2,

130.9, and 128.8. The signal at δ_C = 61.6 is due to oxymethylene carbon. Hence, compound **12** is identified as *o*-dipropyl phthalate.[37]

4.1. Biological Activity of the Extracts and Isolated Compounds. *4.1.1. Antibacterial Activity.* The in vitro antibacterial activity of the extracts and isolated compounds was measured using a disc diffusion assay. The results were expressed in terms of inhibition zone diameter (IZD) and are presented in Table 1.

The methanol extracts of leaves, stems, and roots tested at a concentration of 30 μg/mL showed weak antibacterial activity against the four bacterial pathogens (*S. pyogens*, *S. aureus*, *P. aeruginosa*, and *E. coli*) with an IDZ range of 6.1 ± 0.3 to 9.30 ± 0.20 mm. The result obtained herein for the extract is inferior compared with the literature reports.[38] However, the antibacterial activity reported for the essential oil by Bibiso et al., was found to be in good agreement with our findings.[39] All of the isolated compounds displayed weak antibacterial activity against the tested microorganisms, except for compounds **3**, **4**, and **6**, which showed moderate activity. The best activity was observed for compound **6** against Gram-negative bacteria (*E. coli*, IZD = 13.3 ± 0.5 and 11.3 ± 0.4 mm and *P. aeruginosa*, IZD = 13.5 ±

Table 3. ADME Predictions of the Test Compounds Computed by SwissADME and PreADMET[a]

	absorption			distribution		metabolism					excretion	
	GI ABS	log Kp cm/s	P-gp substrate	BBB permeability (logBB)	log VD (L/kg)	CYP3A4 inhibitor	CYP2D6 inhibitor	CYP2C9 inhibitor	CYP2C19 inhibitor	CYP1A2 inhibitor	TC (log mL/min/kg)	OCT2 substrate
1	low	−2.36	yes	0.769	0.261	no	no	yes	no	no	1.588	no
2	low	−1.65	no	0.815	0.293	no	no	no	no	yes	1.989	no
3	high	−3.09	no	−0.552	−0.06	yes	no	no	no	yes	2.008	no
4	high	−5.39	yes	−0.2	−0.235	no	yes	no	no	no	1.763	no
5	high	−5.84	no	−0.724	−0.044	yes	yes	yes	no	yes	0.764	no
6	high	−5.28	no	0.675	0.182	no	no	no	no	no	0.459	no
7	low	−1.28	yes	−0.939	−1.293	yes	no	no	no	no	0.722	no
8	low	−2.42	yes	−0.995	−0.067	no	no	no	no	no	1.875	no
9	high	−6.49	no	−0.309	−0.014	no	no	no	no	yes	0.768	no
10	high	−6.69	no	−0.456	−0.229	no	no	no	no	yes	0.876	no
11	low	0.71	yes	−0.617	−0.854	no	no	no	no	no	0.748	no
12	high	−5.51	no	0.008	−0.101	no	no	no	yes	yes	0.837	no
CPFX	high	−9.09	yes	−0.425	−0.17	no	no	no	no	no	0.633	no

[a]GI = gastro-intestinal, ABS = absorption, BBB = blood−brain barrier, P-gp = P-glycoprotein, and CYP = cytochrome-P.

0.5 and 11.6 ± 0.4 mm), respectively, compared to ceftriaxone (IZD = 14.1 ± 0.3, 13.8 ± 0.5, 14.4 ± 0.9, and 16.2 ± 0.6, respectively) at concentration of 30 μg/mL. Compounds **4** and **6** displayed IZD of 12.7 ± 0.9 mm and 11.4 ± 0.4 mm against *S. aureus* and *S. pyogens*, respectively, at 30 μg/mL. Hence, the activity displayed by the leaves extract of *A. abyssinica* could be attributed to the presence of compounds **3**, **4**, and **6** in the extract. Literature reports revealed that the leaves of many *Artemisia* species exhibited modest antibacterial activity.[40]

4.1.2. Cytotoxic Activity. Hence, the effect of extracts of *A. abyssinica* was evaluated on breast cancer (MCF-7) cells by the MTT assay, which induced a decrease of cell viability and exerted a cytotoxic effect at a concentration of 20 μg/mL. The percent cell viability of the *n*-hexane and methanol extracts of the leaves of *A. abyssinica* was 54.9 and 16.3%, respectively. The *n*-hexane, EtOAc, and methanol extracts of the stems displayed percent cell viability of 68.6, 74.0, and 92.9%, respectively. Likewise, the EtOAc and methanol root extracts showed percent cell viability of 66 and 34.5%, respectively (Figure 2). Generally, the cytotoxicity activities of the extracts could be attributed to the presence of flavonoids, triterpenes, aromatic compounds, and phenolic constituents in the extracts, showing their activity against the tested cancer cell.

4.1.2.1. Lipinski's and Veber Rules. Lipinski's ROF is one of the most effective tools for predicting new chemical entities' (NCE) drug-likeness.[19] The results are presented in Table 2. Similar to the standard drug, CPFX (hydrochloride), the test compounds **4**, **5**, **6**, **9**, **10**, and **12** comply with the ROF. Whereas all other test compounds showed one or two violations due to their high molecular weight (M.Wt. > 500) and/or lipophilic character (cLogP > 5). Veber's rule,[20] which specifies that the number of rotatable bonds should be ≤ 10 and the TPSA should be ≤140 Å^2 or ≤12 total hydrogen bonds, is a commonly acknowledged technique for predicting the oral bioavailability of NCE. Like CPFX, the test compounds **5**, **6**, **9**, **10**, and **12** comply with Veber's rule. Whereas, the other test compounds showed one violation due to more number of rotatable bonds (>10) as these compounds had open-chain structures. Based on the above two rules, compounds **5**, **6**, **9**, **10**, and **12** appeared to be good oral drug candidates.

4.1.2.2. ADME Studies. The reference drug, CPFX, and the test compounds exhibited high GI absorption except **1**, **2**, **7**, **8**,

and **11** (Table 3). Skin permeability is a measure of how quickly a substance permeates the stratum corneum (Kp). This value is frequently used to emphasize the significance of skin absorption and to quantify the movement of molecules in the outermost layer of the epidermal skin. Lesser the log Kp value, the lower the cutaneous permeability of the molecule.[41] In this study, compared to CPFX, the test compounds showed a higher log Kp value (Table 3), so these compounds might have better skin permeation than CPFX. Increased P-glycoprotein (P-gp) expression in the intestine can limit the absorption of medicines that are P-gp substrates. As a result, bioavailability is diminished, and therapeutic plasma concentrations are not achieved.[42] In the present study, **1**, **4**, **7**, **8**, and **11** and CPFX were predicted to be P-gp substrates.

Blood−brain barrier (BBB) permeability is one of the important parameters that molecules exhibit their action at CNS.[43] It has been suggested that molecules with a logBB value more than 0.3 can easily penetrate the BBB, whereas those with a logBB value less than −1 are not well distributed throughout the brain.[44] Among the test and standard compounds, only **1**, **2**, and **6** showed logBB > 0.3 (Table 3). Therefore, these molecules might have readily crossed the BBB and act on the CNS. The volume of distribution (VD) is the theoretical volume that would be required for a drug's whole dosage to be evenly dispersed to produce a concentration identical to that of blood plasma. If logVD < −0.15, it is considered to be low; if logVD > 0.45, it is considered to be high.[43] Compounds **4**, **7**, **10**, and **11** and CPFX might have less VD, since they showed logVD < −0.15, whereas, other compounds might have moderate VD, since these compounds showed logVD between −0.15 and 0.45 (Table 3).

About 60% of prescribed drugs are metabolized by CYP enzymes, with CYP3A4 accounting for about half of this metabolism, followed by CYP2D6, CYP2C9, and CYP2C19.[45] The CYP3A4 enzyme was inhibited by compounds **3**, **5**, and **7**, suggesting that this enzyme may not have metabolized these compounds. Whereas, CYP2C19 was inhibited only by **12**, and CYP2D6 was inhibited by compounds **4** and **5**. Six of the test compounds inhibited CYP1A2 and only **12** inhibited CYP2C19 (Table 3). The primary transporter for cation influx in renal epithelial cells is organic cation transporter 2 (OCT2). It is involved in the initial stage of renal elimination, which involves
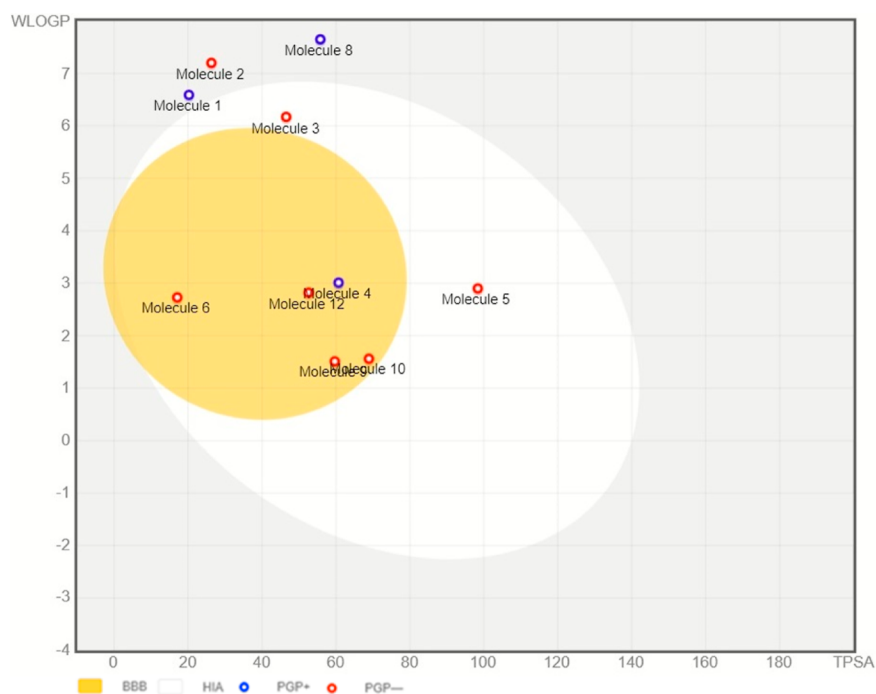
Figure 3. Boiled-egg model for predicting GIT absorption and brain access.

Table 4. Test Compounds Toxicity Prediction Based on Findings by Pro-Tox II

sample	LD$_{50}$ (mg/kg)	toxicity class	organ toxicity				
			hepatotoxicity	carcinogenicity	immunotoxicity	mutagenicity	cytotoxicity
1	1190	4	yes	no	yes	no	no
2	5000	5	no	yes	no	no	no
3	5000	5	no	no	no	no	no
4	20,000	6	no	no	no	no	no
5	5000	5	no	no	yes	no	no
6	4300	5	no	no	no	no	no
7	11,210	6	no	no	yes	no	no
8	1330	4	no	no	no	no	no
9	280	3	no	yes	yes	no	no
10	3800	5	no	no	yes	no	no
11	1000	4	no	no	yes	no	no
12	10,000	6	No	yes	no	no	no
CPFX	2000	4	No	no	no	yes	no

drug molecules being taken up from the blood and entering the proximal tubule cell through the basolateral membrane. According to the study's predictions, none of the compounds were OCT2 substrates.

4.1.2.3. Boiled-Egg Model. The compounds' cLogP and TPSA values were plotted to estimate access to the BBB and human intestinal absorption (HIA) (Figure 3). The egg-shaped plot has been divided into 3 parts, including a white area (HIA), a yellow area (BBB access), and a gray area (no HIA or BBB access). In this prediction, compounds **3** and **5** are in the white area, so these compounds could be absorbed through the intestine, whereas **4**, **6**, **9**, **10**, and **12** are in the yellow area, suggesting that these two compounds may pass through the BBB. Compounds **1**, **2**, and **8** are in the gray area, which indicates no HIA or BBB access (Daina 2016). Compounds **7** and **11** were out of range in this study. Additionally, this model predicted whether those substances are P-gp (PGP) substrates. Blue dots (PGP+) indicate molecules that are substrates of the PGP CNS efflux transporter and could be effluated from the

CNS, whereas red dots (PGP−) indicate substances that are not PGP substrates that could cross and act on the CNS.[46] In this study, compounds **1**, **4**, and **8** had blue dots, suggesting that these compounds are PGP substrates and eventually not acting on the CNS.[47]

4.1.2.4. Toxicity Studies. On a scale of 1 to 6, the degree of toxicity is expressed, with a higher number denoting a lower level of toxicity. This assessment is based on the LD$_{50}$ (mg/kg) value, which represents the dose that kill 50% of the test animals. Among the compounds studied, compounds **4**, **7**, and **12** were predicted to be less or not toxic as they fall under class 6. Compounds **2**, **3**, **5**, **6**, and **10** showed a toxic classification of 5, while compounds **1**, **8**, and **11** exhibited a toxic classification of 4, similar to that of CPFX. Compound **9** appeared to be more toxic, with a toxic classification of 3. Except for compound **1**, none of the tested compounds revealed hepatotoxicity (liver toxicity). All of the compounds also appeared to have no mutagenicity and no cytotoxicity. Except for compounds **2**, **3**, **4**, **6**, **8**, and **12**, the other compounds exhibited immunotoxicity

Table 5. Binding Affinity and Interaction with the Target *E. coli* DNA Gyrase (PDB ID: 6F86)

compd	affinity (kcal/mol)	H-bond	residual amino acid interactions	
			hydrophobic/π-cation/π-anion/ π-alkyl interactions	van der Waals interactions
1	−4.8	Ser121, Val97	Ile94, Ile78	
2	−4.4	Ser121, Val120	Ile94, Ile78	
3	−4.7	Ser121, Val120, Asp49	Ile94, Ile78, Ala47	
4	−5.5	Thr165, Asn46	Ile94, Ile78, Pro79	
5	−6.9	Thr165, Asn46, Arg76	Ile94, Pro79, Glu50	
6	−5.4	Asn46	Ile94, Pro79, Val71, Val43, Ala47	
7	−5.3	Ser121, Val120, Asn46	Ile94, Pro79	
8	−5.4	Ser121, Asn46, Leu98[a]	Ile94, Ile78	
9	−5.8	Thr165, Asn46	Ile94, Ile78, Ala47	
10	−6.7	Asn46, Glu50	Ile78, Ile94, Pro79, Arg76	
11	−5.2	Val120, Ser121	Ile78, Ile94, Ala90, Val93	
12	−6.3	Asn46, Pro79[a]	Ile78, Ile94, Glu50	
CPFX	−7.3	Ser121, Val120, Val97, Leu98	Ile94, Gly119	Glu50, Ile78, Pro79

[a]Carbon hydrogen bond. The binding interactions (3D and 2D) of the isolated compounds and CPFX against *E. coli* DNA gyrase are presented as Supporting Information (Figure S49).

Table 6. Binding Affinity and Interaction with the Target *S. aureus* PK (PDB ID: 3T07)

sample	affinity (kcal/mol)	H-bond	residual amino acid interactions	
			hydrophobic/π-cation/π-anion/ π-alkyl interactions	van der Waals interactions
1	−2.8	Ser362	Ile361, Ala358	
2	−2.9	Ser362	His365, Ile361, Ala358	
3	−3.4	Thr366, Asn369	His365, Ile361, Ala358, Leu370	
4	−3.6	Ser362, Thr366, Asn369	Ile361	
5	−5.0	Ser362, Thr366	His365, Ile361	
6	−3.1	Asn369	His365, Ile361, Leu361	
7	−3.8	Thr366, Asn369	His365, Ile361	
8	−3.3	Ser362, Thr366	His365, Leu370	
9	−4.0	Thr366, Asn369	His365	
10	−4.2	Thr366, Asn369	His365, Leu370	
11	−4.3	Thr366, Asn369, His365	His365, Leu368, Leu344, Lys341	
12	−3.8	Thr366, Asn369	His365, Leu370	
CPFX	−4.9	Ser-362, Thr-366	His365	

(the ability to disrupt the immune system). Only compounds **2**, **9**, and **12** showed carcinogenicity (Table 4).

4.1.2.5. Molecular Docking with DNA Gyrase. DNA gyrase is necessary for the topology and integrity of bacterial DNA during transcription and replication. It is currently regarded as one of the main targets and is present in the majority of pathogenic bacteria in clinical settings.[48,49] Well-known DNA gyrase inhibitors, fluoroquinolones, target the enzymes A subunit.

In this study, *E. coli* DNA gyrase (PDB ID: 6F86) was used as a target, and a fluoroquinoline class of antibacterials, CPFX, was used as a reference control for docking with the target. Binding affinity and interactions with different amino acids are presented in Table 5, and 3D and 2D binding interactions are depicted in Supporting Information; Figure S1. Among the test compounds, compound **5** showed the higher binding affinity (−6.9 kcal/mol), followed by compound **10** (−6.7 kcal/mol) and compound **12** (−6.3 kcal/mol), whereas CPFX showed −7.3 kcal/mol. CPFX formed hydrogen bonding interactions with Ser121, Val120, Val97, and Leu98. Similarly, some of the test compounds (compounds **1**, **2**, **3**, **6**, **7**, **8**, and **11**) showed H-bonding interactions with one or two of these amino acids, whereas other test compounds showed interactions with Thr165 and/or Asn46. CPFX showed residual interactions with Ile94 and Gly119, whereas most of the test compounds showed

interactions with Ile94 and Ile78 along with other amino acids. Only CPFX showed van der Waals interactions, whereas the test compounds did not show van der Waals interactions with any amino acids.

*4.1.2.6. Molecular Docking with *S. aureus* PK.* PK is an essential enzyme found in staphylococci that controls the bacteria's growth, antibiotic resistance, and ability to create biofilms.[50] Moreover, it was discovered to differ structurally from human homologues, making it a potential target for new antimicrobial drugs.[51] Binding affinity and interactions with different amino acids are presented in Table 6, and the 2D and 3D binding interactions are presented as Supporting Information. Among all the compounds, compound **5** showed the highest binding affinity (−5.0 kcal/mol), followed by compound **11** (−4.3 kcal/mol), compound **10** (−4.2 kcal/mol), and compound **9** (−4.0 kcal/mol), whereas CPFX showed binding affinity of −4.9 kcal/mol. CPFX forms H-bonding interactions with Ser362 and Thr366. All the test compounds showed H-bonding interactions with one or two of these amino acids. CPFX showed residual amino acid interactions only with His365. Similarly, the test compounds showed interactions with His365 along with other amino acids, whereas van der Waals interactions were not observed for the standard and test compounds. The binding interactions (3D and 2D) of test

Table 7. Binding Affinity and Interaction with the Target Human TOP2β (PDB ID: 3QX3)

sample	affinity (kcal/mol)	H-bond	residual amino acid interactions	
			hydrophobic/π-cation/π-anion/π-alkyl interactions	van der Waals interactions
1	−3.8	His775	Lys505, Ala779	
2	−3.7	His775, Gly776	Lys505, Ala779	
3	−3.5	His775	Lys505, Ala779, Met782	
4	−3.7	His775, Asp561, Arg729, Lys505		
5	−6.0	His775	Asp561, Glu477, Gly478	
6	−3.4	His775	Lys505	
7	−4.3	His775	Lys505, Ala779	
8	−4.0	His775, Gly776		
9	−4.9	His775, Lys505	Ala779, Asp561	
10	−5.0	His775	Lys505, Glu477, Asp557, Asp559	
11	−5.4	Lys505, Arg729	His775, Ala779, Arg503	
12	−4.4	His775, Gly776	Ala779, His775, Asp561	
EVP	−7.5	His-775, Lys-505, Asp-561, Arg-503	Arg-503, His-775, Glu-522	Gly776, Ala779, Arg729, Asp559, His774, Glu477

compounds and CPFX against *S. aureus* PK are presented as Supporting Information (Figure S50).

4.1.2.7. Molecular Docking with Human Topoisomerase IIβ. Topoisomerase II (TOP2) catalyzes the relaxing and unwinding of double-stranded DNA, which is essential for DNA replication, transcription, and repair.[52] Recent studies showed that TOP2β is an important target for many anticancer agents, including etoposide (EVP). Binding affinity and interactions with different amino acids are presented in Table 7, and the 2D and 3D binding interactions are presented as Supporting Information. EVP showed a binding affinity of −7.5 kcal/mol, whereas all of the test compounds showed a lesser binding affinity. Compound **5** showed a binding affinity of −6.0 kcal/mol, followed by compound **11** (−5.4 kcal/mol), compound **10** (−5.0 kcal/mol), and compound **11** (−4.9 kcal/mol). EVP showed H-bonding interactions with His-775, Lys-505, Asp-561, and Arg-503, while the test compounds showed interactions with one or more of these amino acids. EVP showed residual amino acid interactions with Arg-503, His-775, and Glu-522, whereas most of the test compounds showed interactions with different amino acids. Only EVP showed van der Walls interactions, whereas the test compounds did not show van der Walls interactions with any amino acids. The binding interactions (3D and 2D) of test compounds and EVP against human topoisomerase IIβ are included as Supporting Information (Figure S51).

5. CONCLUSIONS

Column chromatographic fractionation of the extracts of *A. abyssinica* has led to the isolation of 12 compounds, of which compounds **1**, **3**, **4**, **5**, and **7-11** are new to the genus *Artemisia*. All the crude extracts displayed weak antibacterial activity with IZD ranges of 6.1 ± 0.3 to 9.30 ± 0.20 mm at 30 µg/mL. Compound **6** had the best antibacterial activity against *E. coli* (IZD = 13.30 ± 0.50 mm) and *P. aeruginosa* (IZD = 13.50 ± 0.50 mm) compared to ceftriaxone (IZD = 14.1 ± 0.3 and 13.8 ± 0.5 against *E. coli* and *P. aeruginosa*, respectively). Therefore, it can be concluded that the activity displayed by the leaves extract of *A. abyssinica* could be attributed to the presence of compounds **3**, **4**, and **6** in the extract. The in silico molecular docking analysis against DNA gyrase B revealed that compound **5** showed a higher binding affinity (−6.9 kcal/mol), which is comparable with that of CPFX (−7.3 kcal/mol). Similarly,

compound **5** had a better result compared with CPFX (−4.9 kcal/mol) against *S. aureus* PK with a binding affinity of −5.0 kcal/mol. The binding affinities of the isolated compounds against human topoisomerase inhibitors IIβ revealed that compound **5** showed a binding affinity of −6.0 kcal/mol, followed by **11** (−5.4 kcal/mol), **10** (−5.0 kcal/mol), and **11** (−4.9 kcal/mol). Similar to CPFX, compounds **4**, **5**, **6**, **9**, **10**, and **12** comply with Lipinski's ROF. The effect of the extracts of *A. abyssinica* was evaluated against breast cancer (MCF-7) cell lines using the MTT assay. The extracts induced a decrease in cell viability and exerted a cytotoxic effect at a concentration of 20 µg/mL. Therefore, the cytotoxicity, antibacterial activities, and in silico molecular docking analysis displayed by the constituents validate the traditional uses of the plant against microbial infections and cancer.

■ ASSOCIATED CONTENT

ⓢ Supporting Information

The Supporting Information is available free of charge at https://pubs.acs.org/doi/10.1021/acsomega.4c01096.

■ AUTHOR INFORMATION

Corresponding Author

Yadessa Melaku − *Department of Applied Chemistry, Adama Science and Technology University, Adama, Ethiopia;* ⓞ orcid.org/0000-0003-2599-0517; Email: yadessa.melaku@astu.edu.et

Authors

Dawit Tesfaye − *Department of Applied Chemistry, Adama Science and Technology University, Adama, Ethiopia*

Milkyas Endale − *Traditional and Modern Medicine Research and Development Directorate, Armauer Hansen Research Institute, Addis Ababa 1165, Ethiopia*

Venkatesha Perumal Ramachandran − *Department of Applied Chemistry, Adama Science and Technology University, Adama, Ethiopia;* ⓞ orcid.org/0000-0001-5368-1637

Emebet Getaneh − *Department of Applied Biology, Adama Science and Technology University, Adama 311-2118, Ethiopia*

Guta Amenu − *Department of Applied Biology, Adama Science and Technology University, Adama 311-2118, Ethiopia*

Leta Guta − *Department of Applied Biology, Adama Science and Technology University, Adama 311-2118, Ethiopia*

Taye B. Demissie − *Department of Chemistry, University of Botswana, Gaborone P/Bag 00704, Botswana;* ● orcid.org/0000-0001-8735-4933

Japheth O. Ombito − *Department of Chemistry, University of Botswana, Gaborone P/Bag 00704, Botswana*

Rajalakshmanan Eswaramoorthy − *Department of Biomaterials, Saveetha Dental College and Hospitals, Saveetha Institute of Medical and Technical Sciences (SIMATS), Saveetha University, Chennai 600 077, India;* ● orcid.org/0000-0002-8331-2100

Complete contact information is available at:
https://pubs.acs.org/10.1021/acsomega.4c01096

Notes

The authors declare no competing financial interest.

■ REFERENCES

(1) Rustaiyan, A.; Masoudi, S. Chemical Constituents and Biological Activities of Iranian Artemisia species. *Phytochem. Lett.* **2011**, *4*, 440−447.

(2) Alesaeidi, S.; Miraj, S. A Systematic Review of Anti-Malarial Properties, Immunosuppressive Properties, Anti-Inflammatory Properties, and Anti-Cancer Properties of *Artemisia Annua*. *Electron. Physician* **2016**, *8*, 3150−3155.

(3) Vallès, J.; Garcia, S.; Hidalgo, O.; Martín, J.; Pellicer, J.; Sanz, M.; Garnatje, T. Biology, Genome Evolution, Biotechnological Issues and Research Including Applied Perspectives in Artemisia (Asteraceae). *Adv. Bot. Res.* **2011**, *60*, 349.

(4) Ayenew, K. D.; Ayalew, A.; Wondmkun, Y. T.; Tsige, A. W.; Wolde, A.; Sewale, Y.; Belihu, G. D.; Fekade, E.; Habteweld, H. A. *In vivo* Immunomodulatory Activities of Essential Oils of Artemisia abyssinica and *Lepidium sativum* in Mice. *ImmunoTargets Ther.* **2024**, *13*, 15−27.

(5) Abdu, N.; Alebachew, Y. Diuretic Activity of the Hydroalcoholic Extracts of Rhizomes and Leaves of *Artemisia abyssinica* Sch. Bip. ex A. Rich: *In silico* and *in vivo* Study. *Scr. Med.* **2024**, *55* (1), 63−70.

(6) Sharifi-Rad, M.; Roberts, T. H.; Matthews, K. R.; Bezerra, C. F.; Morais-Braga, M. F. B.; Coutinho, H. D.; Sharopov, F.; Salehi, B.; Yousaf, Z.; Sharifi-Rad, M.; et al. Ethnobotany of the genus Taraxacum-Phytochemicals and Antimicrobial activity. *Phytother. Res.* **2018**, *32* (11), 2131−2145.

(7) Ayele, A. G.; Kawet, J. S. Evaluations of the in vivo Laxative Effects of Aqueous Leaf and Stem Extracts of *Artemisia Abyssinica* in Mice. *J. Exp. Pharmacol.* **2024**, *16*, 135−142.

(8) Farmer, P. J.; Frenk, J.; Knaul, F. M.; Shulman, L. N.; Alleyne, G.; Armstrong, L.; Atun, R.; Blayney, D.; Chen, L.; Feachem, R.; et al. Expansion of cancer care and control in countries of low and middle income: a call to action. *Lancet* **2010**, *376*, 1186−1193.

(9) Hanahan, D.; Weinberg, R. A. The Hallmarks of Cancer. *Cell* **2000**, *100*, 57−70.

(10) Wood, J. R. I. *A Handbook of the Yemen Flora*; Royal Botanic Garden: Kew, UK, 1997; Vol. *300*.

(11) Petchiappan, A.; Chatterji, D. Antibiotic resistance: Current perspectives. *ACS Omega* **2017**, *2*, 7400−7409.

(12) Bray, F.; Laversanne, M.; Weiderpass, E.; Soerjomataram, I. The ever-increasing importance of Cancer as a leading cause of premature death worldwide. *Cancer* **2021**, *127*, 3029−3030.

(13) Tariku, Y.; Hymete, A.; Hailu, A.; Rohloff, J. Essential-Oil Composition, Antileishmanial, and Toxicity Study of Artemisia abyssinica and Satureja punctata ssp. punctata from Ethiopia. *Chem. Biodiversity* **2010**, *7*, 1009−1018.

(14) Asfaw, N.; Demissew, S. *Aromatic Plants of Ethiopia*; Shama Books: Addis Ababa, 2009.

(15) Rea, T.; Berhanu, A.; Sab, Y. Bovine Tuberculosis and Brucellosis Prevalence in cattle from selected cooperative in Arsi zone Oromia region, Ethiopia. *BMC Vet. Res.* **2013**, *9*, 163.

(16) El-Shemy, H. A.; Aboul-Enein, A. M.; Aboul-Enein, K. M.; Fujita, K. Willow leaves' extracts contain antitumor agents effective against three cell types. *PLoS One* **2007**, *2*, 178.

(17) Bauer, A.; Kirby, W.; Sherris, C.; Turck, M. Antibiotic susceptibility testing by a standardized single disk method. *Am. J. Clin. Pathol.* **1966**, *45* (4_ts), 493−496.

(18) Lipinski, C. A.; Lombardo, F.; Dominy, B. W.; Feeney, P. J. Experimental and Computational approaches to estimate solubility and permeability in drug discovery and development settings. *Adv. Drug Deliv. Rev.* **1997**, *23* (1−3), 3−25.

(19) Veber, D. F.; Johnson, S. R.; Cheng, H. Y.; Smith, B. R.; Ward, K. W.; Kopple, K. D. Molecular properties that influence the oral bioavailability of drug candidates. *J. Med. Chem.* **2002**, *45* (12), 2615.

(20) Daina, A.; Michielin, O.; Zoete, V. SwissADME: a free web tool to evaluate pharmacokinetics, drug-likeness and medicinal chemistry friendliness of small molecules. *Sci. Rep.* **2017**, *7*, 42717.

(21) Lee, S. K.; Lee, I. H.; Chang, G. S.; Chung, J. E.; Tai, N. K. The PreADME Approach: Web-based program for rapid prediction of physicochemical, drug absorption and drug-like properties. In *Euro QSAR 2002 - Designing Drugs and Crop Protectants: Processes Problems and Solutions*; ResearchGate GmbH., 2002; Vol. 23, pp 418−420.

(22) Banerjee, P.; Eckert, A. O.; Schrey, A. K.; Preissner, R. ProTox-II: a webserver for the prediction of toxicity of chemicals. *Nucleic Acids Res.* **2018**, *46*, 257−263.

(23) Frisch, G.; Trucks, H.; Schlegel, G.; Scuseria, M.; Robb, J.; Cheeseman, R.; Fox, D. J. *Gaussian 09*, Revision C. 01; Gaussian, Inc.: Wallingford, CT, 2009.

(24) Damasceno, M. V.; Cunha, A. R.; Provasi, P. F.; Pagola, G. I.; Siqueira, M.; Manzoni, V.; Gester, R.; Canuto, S. Modulation of the NLO properties of p-coumaric acid by the solvent effects and proton dissociation. *J. Mol. Liq.* **2024**, *394*, 123587.

(25) Pawar, S. S.; Rohane, S. H. Review on Discovery Studio: An important Tool for Molecular Docking. *Asian J. Res. Chem.* **2021**, *14*, 1−3.

(26) Trott, O.; Olson, A. J. AutoDock Vina: improving the speed and accuracy of docking with a new scoring function, efficient optimization and multithreading. *J. Comput. Chem.* **2010**, *31*, 455−461.

(27) Perumal, V. R.; Revathi, R. Anxiolytic-like activity of serotonin-3 receptor antagonist: In-silico molecular modeling, drug-likeness and evaluation of anxiolytic activity *Songklanakarin. J. Sci. Technol.* **2022**, *44* (3), 646−652.

(28) Nguyen, N. T.; Nguyen, T. H.; Pham, T. N. H.; Huy, N. T.; Bay, M. V.; Pham, M. Q.; Nam, P. C.; Vu, V. V.; Ngo, S. T. AutoDock Vina Adopts More Accurate Binding Poses but Autodock4 Forms Better Binding Affinity. *J. Chem. Inf. Model.* **2020**, *60* (1), 204−211.

(29) Gribanova, S. V.; Kharitonov, Yu.; Dzhabarov, D. N.; Rudenko, B. A.; Yanotovskii, M. T. Gas-chromatographic identification of impurities in intermediate products of the synthesis of vitamin E based on the additive scheme of calculation of retention indices. *Zh. Anal. Khim.* **1991**, *45*, 510.

(30) Knothe, G. *Agricultural Research Service*; U.S. Department of Agriculture, National Center for Agricultural Utilization Research: N. University St, Peoria, IL 61604, USA, 1815.

(31) Wang, Z. H.; Li, Q.; Huang, M.; Xu, P. F.; Yang, L. P.; Zhai, Y. Y.; Zhang, Z. Z.; Zhang, W. K.; Niu, C.; Wang, H. Chemical constituents of *Callicarpa macrophylla. Chem. Nat. Compd.* **2020**, *56*, 1125−1127.

(32) Sichaem, J.; Inthanon, K.; Funnimid, N.; Phontree, K.; Phan, H.-V.-T.; Tran, T.-M.-D.; Niamnont, N.; Srikittiwanna, K.; Sedlak, S.; Duong, T. H. Chemical Constituents of the Stem Bark of *Bombax ceiba*. *Chem. Nat. Compd.* **2020**, *56*, 909−911.

(33) Darmawan, A.; Kosela, S.; Kardono, L. B. S.; Syah, Y. M. Scopoletin, a Coumarin derivative compound isolated from *Macaranga gigantifolia*. *J. Appl. Pharm. Sci.* **2012**, *2* (12), 175−177.

(34) Kurdekar, R. R.; Hegde, G. R.; Kulkarni, M. V.; Mulgund, G. S. Isolation and Characterization of scopoletin- an anticancerous compound from the bark of Hymenodictyon obovatum Wall. *Int. J. Pharm. Phytopharm. Res.* **2012**, *3* (6), 469−471.

(35) Piironen, V.; Lindsay, D. G.; Miettinen, T. A.; Toivo, J.; Lampi, A. M. Plant sterols: biosynthesis, biological function and their importance to human nutrition. *J. Sci. Food Agric.* **2000**, *80*, 939−966.

(36) Sun, S.; Shen, J.; Li, B.; Geng, J.; Ma, L.; Qi, H.; Zhang, A.; Zhao, Z. The spatiotemporal distribution and potential risk assessment of 19 phthalate acid esters in wastewater treatment plants in China. *Environ. Sci. Pollut. Res.* **2021**, *28* (47), 67280−67291.

(37) Youssef, M. M.; Mahmoud, A. A.; Al-Faiyz, Y. S. Antimicrobial and Antioxidant Activities of Artemisia abyssinica Extracts and DNA Degradation Effects. *Asian J. Biochem.* **2014**, *10* (1), 31−41.

(38) Bibiso, M.; Anza, M.; Tadesse, T. Essential Oils Composition, Antibacterial Activity and Toxicity Study of Artemisia Species Growing in Ethiopia. *Trad. Integr. Med.* **2022**, *7* (4), 444−451.

(39) Hanscheid, T.; Hardisty, D. W. How "resistant" is artimisinin resistant malaria? - The risks of ambiguity using the term "resistant" malaria. *Travel Med. Infect. Dis.* **2018**, *24*, 23−24.

(40) Zeng, R.; Deng, J.; Dang, L.; Yu, X. Correlation between the structure and skin permeability of compounds. *Sci. Rep.* **2021**, *11*, 10076.

(41) Elmeliegy, M.; Vourvahis, M.; Guo, C.; Wang, D. D. Effect of P-glycoprotein (P-gp) Inducers on Exposure of P-gp Substrates: Review of Clinical Drug-Drug Interaction Studies. *Clin. Pharmacokinet.* **2020**, *59*, 699−714.

(42) Kadry, H.; Noorani, B.; Cucullo, L. A blood-brain barrier overview on structure, function, impairment, and biomarkers of integrity. *Fluids Barriers CNS* **2020**, *17*, 69.

(43) Pires, D. E. V.; Blundell, T. L.; Ascher, D. B. pkCSM: Predicting Small-Molecule Pharmacokinetic and Toxicity Properties Using Graph-Based Signatures. *J. Med. Chem.* **2015**, *58* (9), 4066−4072.

(44) Esteves, F. J.; Rueff, J.; Kranendonk, M. The Central Role of Cytochrome P450 in Xenobiotic Metabolism A Brief Review on a Fascinating Enzyme Family. *J. Xenobiot.* **2021**, *11* (3), 94−114.

(45) Daina, A.; Michielin, O.; Zoete, V. SwissADME: a free web tool to evaluate pharmacokinetics, drug-likeness and medicinal chemistry friendliness of small molecules. *Sci. Rep.* **2017**, *7*, 42717.

(46) Drwal, M. N.; Banerjee, P.; Dunkel, M.; Wettig, M. R.; Preissner, R. ProTox: a web server for the in-silico prediction of rodent oral toxicity. *Nucleic Acids Res.* **2014**, *42*, 53−58.

(47) Janupally, R.; Medepi, B.; Brindha Devi, P.; Suryadevara, P.; Jeankumar, V. U.; Kulkarni, P.; Yogeeswari, P.; Sriram, D. Design and Biological Evaluation of Furan/Pyrrole/Thiophene-2-carboxamide Derivatives as Efficient DNA GyraseB Inhibitors of Staphylococcus aureus. *Chem. Biol. Drug Des.* **2015**, *86*, 918−925.

(48) Narramore, S.; Maxwell, S.; Lawson, A.; Fishwick, D. M.; Colin, W. G. New insights into the binding mode of pyridine-3-carboxamide inhibitors of E. coli *DNA gyrase. Bioorg. Med. Chem.* **2019**, *27*, 3546−3550.

(49) Vasu, D.; Sunitha, M.; Srikanth, L.; Swarupa, V.; Prasad, U. V.; Sireesha, K.; Yeswanth, S.; Kumar, P. S.; Venkatesh, K.; Chaudhary, A.; et al. *In staphylococcus aureus* the regulation of pyruvate kinase activity by serine/threonine protein kinase favors biofilm formation. *Biotech* **2015**, *5*, 505−512.

(50) Akunuri, R.; Unnissa, T.; Vadakattu, M.; Bujji, S.; Mahammad Ghouse, S.; Madhavi Yaddanapudi, V.; Chopra, S.; Nanduri, S. Bacterial *Pyruvate Kinase*: A New Potential Target to Combat Drug-Resistant *Staphylococcus aureus* Infections. *ChemistrySelect* **2022**, *7*, 1−15.

(51) Delgado, J. L.; Hsieh, C.; Chan, N.; Hiasa, H. Topoisomerases as anticancer targets. *Biochem. J.* **2018**, *475* (2), 373−398.

(52) Farouk, F.; Elmaaty, A. A.; Elkamhawy, A.; Tawfik, H. O.; Alnajjar, R.; Abourehab, M. A. S.; Saleh, M. A.; Eldehna, W. M.; Al-Karmalawy, A. A. Investigating the potential anticancer activities of antibiotics as topoisomerase II inhibitors and DNA intercalators: *in vitro*, molecular docking, molecular dynamics, and SAR studies. *J. Enzyme Inhib. Med. Chem.* **2023**, *38* (1), 1−22.